ESKİŞEHİR TECHNICAL UNIVERSITY JOURNAL OF SCIENCE AND TECHNOLOGY
A- APPLIED SCIENCES AND ENGINEERING

2023, 24(3), pp. 207-215, DOI:10.18038/estubtda.1335496

RESEARCH ARTICLE

FABRICATION OF A NOVEL FeB-B_4C COMPOSITE POWDER AND EVALUATING ITS POTENTIAL FOR ENERGY STORAGE APPLICATIONS

Suna AVCIOĞLU

Department of Metallurgical and Materials Engineering, Faculty of Chemistry and Metallurgy, Yıldız Technical University, Istanbul, Turkey

ABSTRACT

The development of energy storage devices is critical for humanity to declare its independence from fossil fuels. Supercapacitors and batteries are rapidly growing technologies. Nevertheless, their current progress is still insufficient to meet global demand. Therefore, advances in new generation and tailored materials for energy storage applications are urgently needed. Herein, for the first time, a novel composite of FeB-B_4C powder was synthesized by a one-pot sol-gel technique, and its potential as an active material for electrodes in energy storage devices was investigated. The phase analysis showed that a composite powder containing 91±5% B_4C and 9±5% FeB was obtained without unwanted excess phases such as graphite, boron, or iron oxide. Scanning electron microscopy images of the composite powder revealed the formation of elongated boron carbide particles connected with spherical iron boride ones. The size of the boron carbide particles was found to be in the range of 1 to 10 µm, while the iron boride particles were formed in the submicron range. The synthesized composite's electrochemical properties were investigated using a three-electrode set-up. Cyclic voltammetry (CV) and galvanostatic charge/discharge tests (GCD) were employed. The results obtained indicate the pseudocapacitive behavior of the electrodes with a specific capacitance of 8.28 F/g.

Keywords: Iron boride, Boron carbide, Composite, Energy storage, Supercapacitor

1. INTRODUCTION

Pollution and global warming are some of the problems associated with modern society's dependence on fossil fuels due to energy shortages and rising fuel costs [1]. As well as the production of renewable energy, the storage of produced energy is one of the obstacles to reducing dependence on fossil fuels [2]. With the rapid development of the industry, the demand for high-capacity energy storage devices powered by green energy has become increasingly crucial. In terms of environmental impact and resource sustainability, supercapacitors are expected to have a great impact on the transition to greener energy consumption [3].

In recent research progress, the pseudocapacitive or battery type materials (metal sulfides, metal nitrides and metal carbides) have been effectively studied for supercapacitor electrodes due to the existence of their unique redox mechanism [4]. Many transition metal carbides such as, SiC, TiC, V_4C_3, WC, MoC and B_4C have attracted attention for energy storage applications [5]. SiC nanocauliflowers (NCs) were investigated by Amit Sanger et al. as an electrode material for supercapacitors, which increased the high specific capacitance of SiC NCs up to about 300 F/g and produced symmetric devices that delivered high energy (31.43 Wh/kg) and power density (18.8 kW/kg) with good cyclic stability (94%) at 1 M Na_2SO_4 [4]. Two-dimensional vanadium carbide as super capacitor electrode material with aqueous electrolyte was studied by Qingmin shan et al., which achieved the excellent specific capacitance of 487 F/g [5]. Joseph Halim et al., demonstrated the large-scale synthesis and delamination of 2D Mo_2CT electrodes in supercapacitors, capacitances as high as 700 F cm^{-3} and high-capacity retention

*Corresponding Author: suna.avcioglu@yildiz.edu.tr
Received:01.09.2023 Published:22.09.2023

about 10,000 cycles. Besides Mo_2CTx tested the electrode material for Li-ions achieved the reversible capacities of 250 mAh/g [6].

Among the carbide materials, boron carbide (B_4C) is a semiconductor with high chemical resistance [7]. Besides, it has many unique properties that can be useful for energy storage devices, such as high thermal stability, high melting point, low density, and low thermal expansion coefficient [8]. For these reasons, boron carbide (B_4C) has been used in a number of electrochemical energy storage systems, including zinc-air, vanadium redox flow, lithium-oxygen, and lithium-sulfur batteries [9–12]. Wen-Bin Luo et al. could synthesize B_4C nanowires from carbon nanotubes, and they utilized B_4C nanowires as a novel bifunctional electrocatalyst in battery applications [13]. They also reported that B_4C nanowire-based electrodes could be operated up to 2.2 V voltage even after 120 cycles. B_4C nanowires grown in situ on carbon nanofibers (B_4C@CNF) were used by Liu Luo et al. to fabricate a novel cathode substrate, which also achieved 9 mAh/cm^2 areal capacity and excellent capacity retention of 80% after 500 cycles [14]. In addition, Chang et al. showed that the core-shell structure B_4C@C could potentially be an electrode material for all solid-state micro-supercapacitors [15]. In our recent study, we demonstrate that the morphological differences of boron carbide particles influence the electrochemical performance of supercapacitor electrodes made of these particles [16]. So, as indicated in previous studies boron carbide has a great potential for use in energy storage devices. Nevertheless, boron carbide lacks electrical conductivity, and its' slower ionic transport kinetics need to be enhanced to improve its electrochemical performance.

Recently, metal borides have been proposed as co-catalyst for photocatalysis and electrocatalysis because of their charge-transfer enhancement [17–19]. Moreover, the electrochemical properties of some of the metal borides such as TiB, VB, and CoB have been tested for energy storage applications [20,21]. In this study, for the first time in the literature, FeB-B_4C composite powder was synthesized, and its electrochemical properties were investigated. The phase content and morphological features of the composite powder, as well as the charge storage mechanism and performance of the electrodes were revealed and discussed.

2. EXPERIMENTAL

2.1. Synthesis and Characterization of Composite Particles

For the synthesis of iron boride-boron carbide composite particles, analytical grade starting chemicals were purchased from Merck and used without additional purification. All solid starting materials were directly added to glycerin according to the molar ratio given in Table 1. Using a hot plate, the mixture was vigorously magnetic stirred in an oil bath to ensure homogeneous heat distribution. The temperature of the mixture was then gradually increased over an hour to 150°C, where it remained for another hour under vigorous magnetic stirring (450 rpm). After this process, the formed gel was poured into alumina crucibles and cooled to room temperature. Then the gel was calcinated at 675 °C for 2 hours using a muffle furnace to burn off extra carbon. Finally, the calcined product was subjected to a final heat treatment at 1500 °C for 5 hours in a tube furnace under argon (500 ml/min) to obtain composite particles.

Table 1. Molar ratios of starting chemicals.

Glycerin ($C_3H_8O_3$)	**Tartaric Acid ($C_4H_6O_6$)**	**Boric Acid (H_3BO_3)**	**Iron (III) Nitrate ($Fe(NO_3)_3.9H_2O$)**
1 mol	0.25 mol	1 mol	0.25 mol

The phases present in the synthesized powder were analyzed by X-ray diffraction technique (XRD, Bruker D2 Phaser) using Cu Kα radiation (λ = 1.540 Å, 30 kV, and 10 mA) in the range of 10° to 80° with a scanning speed of 0.5°/min. Scanning electron microscopy (SEM, Zeiss EVO LS 10) was used

to examine the particle morphology. Elemental point analysis (EDS-Thermo scientific energy dispersive X-ray detector) was performed to examine the elemental distribution.

2.2. Fabrication of Electrodes and Electrochemical Measurements

To fabricate a working electrode, firstly, a fine paste was prepared by mixing 0.085g of as-synthesized powder, 0.01g C65 conductive carbon black, and 0,005 g poly (vinylidene fluoride) binder with 0.025 mL of NMP (N,N-dimethyl pyrrolidinone) solution. The mixture was placed in a 15 mL glass bottle with a closed lid, and to obtain a homogeneous mixture magnetic stirring was applied at room temperature for 24 hours. The obtained fine mixture was poured onto a nickel foam substrate (1 × 1 cm^2). The coated substrate was then allowed to dry for 24 hours at 80 °C before being employed as a working electrode in all electrochemical experiments. The substrate was coated with 10 mg of active material.

A potentiostat/galvanostat (Metrohm-Vionic) electrochemical workstation was used to examine the electrochemical characteristics of the electrode at room temperature (~25 °C). A three-electrode setup with an aqueous 6 M KOH solution as the electrolyte was used for all electrochemical tests. In the assembled cell, the fabricated electrode containing synthesized particles acts as the working electrode, a Pt spring as the counter electrode, and Ag/AgCl as the reference electrode. Cyclic voltammetry (CV) was performed for different scan rates of 5, 10, 25, 50, 75, and 100 mVs-1. Galvanostatic charge/discharge testing was performed at different charge/discharge current densities (0.5, 1, and 2 Ag-1) in the constant potential window from 0 to 0.4 V.

3. RESULTS AND DISCUSSION

The phase pattern of as-synthesized powders provided by XRD analysis is shown in Figure 1. The pattern indicates that synthesized powder does not contain any amorphous phase, like amorphous carbon. Phase determination carried out by using HighScore Software shows that the powder contains two crystalline phases. The main phase was found to be boron carbide (CoD: 96-223-5963) with a 91±5% ratio. The observed secondary phase was indexed as iron boride (CoD: 96-101-0478) with a 9±5% ratio. Besides these two crystalline phases, no other residual oxide phase, such as boron oxide or iron oxide, was not observed.

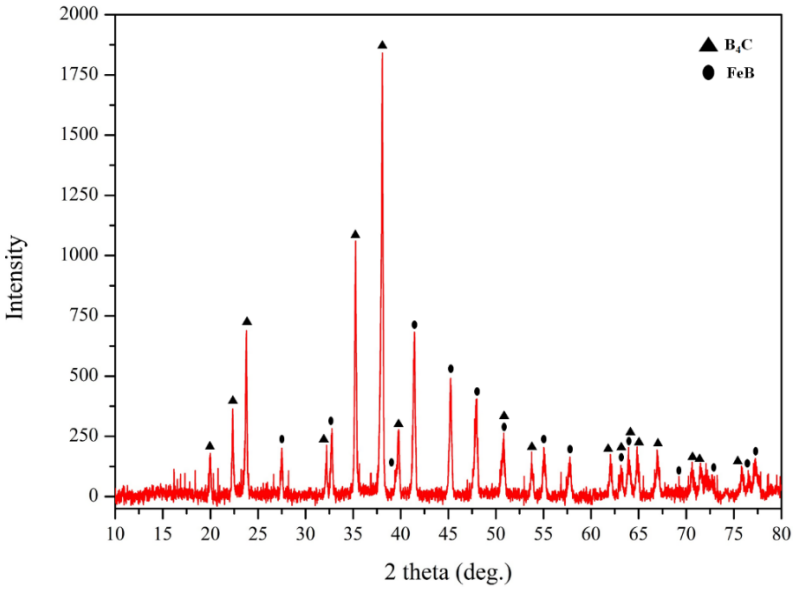

Figure 1. The XRD pattern of as-synthesized powder.

The secondary electron SEM image of the synthesized powder is presented in Figure 2-a. The image shows that most of the particles have elongated complex-shaped morphology. Besides, the surface texture of the particles is observable from the secondary electron SEM image (Figure 2-a). Straight-line marks on the surface of the particles were detected and highlighted with red arrows in Figure 2-a. The line-shaped marks originated because of non-completed stacked crystalline layers of boron carbide, and the marks indicate that the particles were grown via the lateral growth mechanism. The lateral growth of the particles generally results in the formation of particles with a high aspect ratio. Thus, the observed elongated complex-shaped morphology should be related to the dominant growth mechanism in the formation of particles during the final heat treatment stage. The approximate size of the particles was measured from SEM images using Image-J software. It is seen that the size of elongated complex-shaped particles is in the range of 1 to 10 µm. Furthermore, in addition to the micron-sized particles, sub-micron-sized particles with spherical morphology were observed, and these particles were emphasized with red circles in Figure 2-a. Moreover, spherical particles are generally seen as consolidated on the tip of the elongated ones. To reveal the chemical differences between these two types of particles, a backscattered SEM image was obtained and EDX analysis was carried out (Figures 2-b to d). The backscattered SEM image reveals that sub-micron-sized spherical particles appear brighter than elongated complex-shaped ones. This observation is evident that the iron boride phase forms the sub-micron-sized spherical particles. EDX analysis results are presented in Figures 2-c and d, also confirming that the sub-micron-sized spherical particles contain a high amount of iron (EDX-point 1). On the contrary, no iron was detected on EDX-point 2. Moreover, it's known that metal additives promote the uniaxial growth of carbides and nitrides [22,23]. So, it can be concluded that during the final heat treatment, iron boride enhances the lateral growth of boron carbide and particles formed in elongated complex-shaped morphology, unlike boron carbide particles' well-known polyhedral equiaxed morphology [24–26].

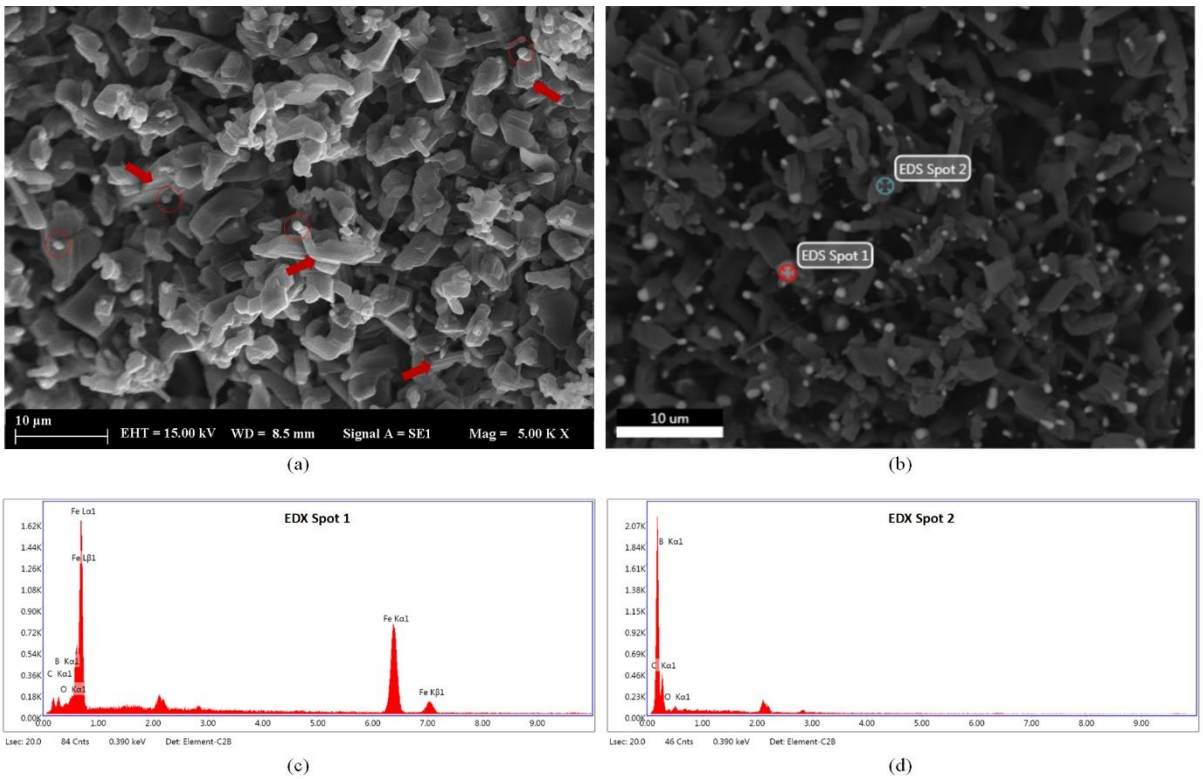

Figure 2. The scanning electron microscopy images and elemental point analysis results of synthesized powder. (a) secondary electron image, (b) backscattered electron image and EDS points, (c) elemental composition of point 1, and (d) elemental composition of point 2.

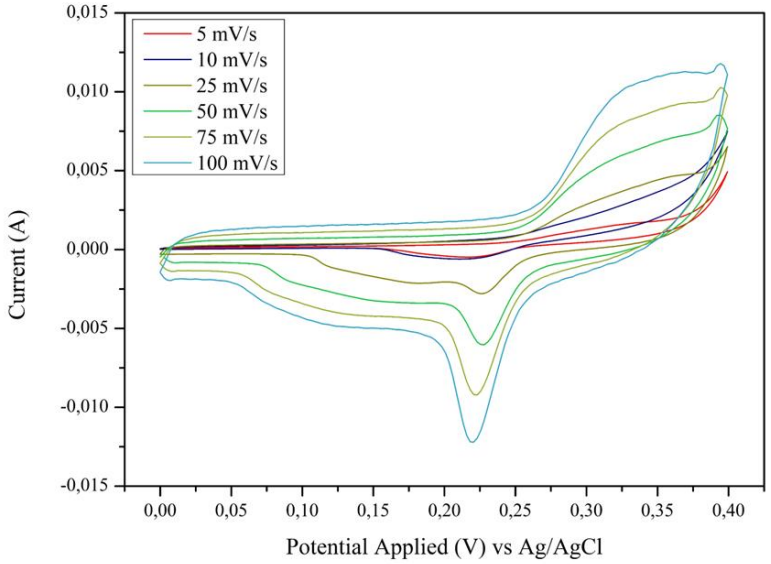

Figure 3. Cyclic voltammetry (CV) curves of the FeB-B_4C electrode at different scan rates in the range of 5 to 100 mV/s.

In order to evaluate the storage mechanism of the synthesized powder-based FeB-B_4C composite electrode, cyclic voltammetry (CV) analysis was performed. Figure 3 shows the cyclic voltammograms of the electrode recorded at different scan rates between 5 and 100 mV/s over a potential working window of 0-0.4 V in an aqueous solution of 6 M KOH. The obtained CV curves exhibit an identical profile, showing the film's strong reversibility in the 6 M KOH electrolyte. It is seen that the area under CV curves increases with the scan rate. This phenomenon can be explained by limited diffusion at high scan rates, so higher current occurs, and higher current results in an increase in CV curve area [27]. Moreover, clear oxidation and reduction peaks were determined in the CV curves, demonstrating the electrode's pseudocapacitive behavior. In addition, a slight shift in the potential positions of both the oxidation and reduction peaks was observed with increasing scan rate. This observation may correspond to the electrodes' low polarization [28].

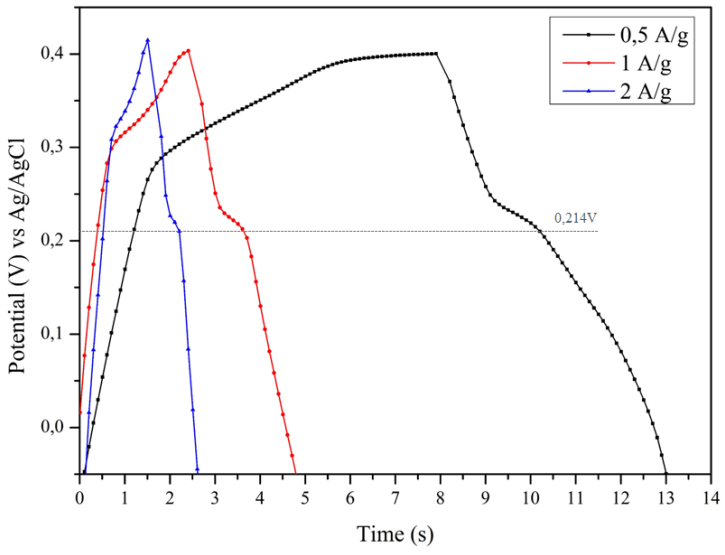

Figure 4. Galvanostatic charge-discharge (GCD) curves of the FeB-B_4C electrode at current densities of 0.5 A/g, 1 A/g, and 2 A/g.

To assess the performance of the electrode materials for energy storage devices, galvanostatic charge-discharge (GCD) was employed. The GCD profiles obtained at various scan rates are displayed in Figure 5 for comparison. It can be seen that the discharge curves are not linear and exhibit a potential slope just above 0.214 V, suggesting the presence of pseudo-capacitance behavior, which is consistent with the CV measurements. Equation 1 is used to calculate the specific capacitance of electrode materials from galvanostatic discharge curves.

$$C_s = \frac{\Delta T \times i}{\Delta V \times m} \tag{1}$$

$\boldsymbol{i}$: current (A), $\Delta \boldsymbol{T}$: the discharge time (s), $\Delta \boldsymbol{V}$: potential window (V), $\boldsymbol{m}$: mass of active material (g)

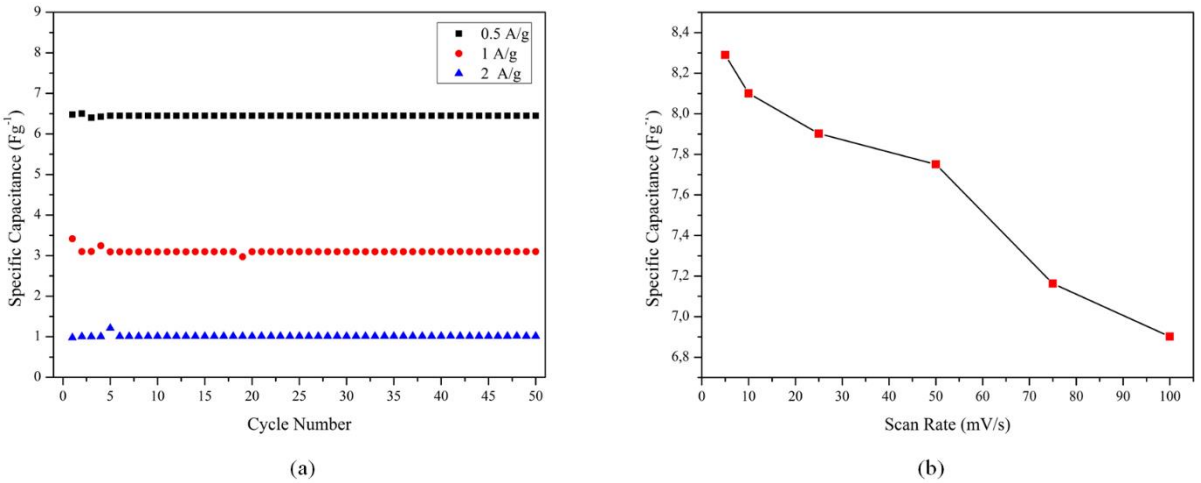

Figure 5. Comparative specific capacitance values of the FeB-B_4C electrode. (a) specific capacitance values calculated from GCD curves in a function of cycle number and current densities, (b) specific capacitance values calculated from CV curves in a function of scan rate.

The specific capacitance values obtained from the GCD curves for different scan rates and during 50 cycles are shown in Figure 5-a. It can be seen that the specific capacitance values are constant up to 50 cycles, indicating the stability of the electrodes. Moreover, the calculated specific capacitance value at 0.5 A/g is 6.5 F/g, decreasing to 1 F/g with increasing current density to 2 A/g. The decrease in specific capacitance at high current density is likely caused by the electrolyte ions' adverse accessibility to the electrode's core active sites [29]. Determination of the specific capacitance values from GCD curves is a good approach to characterize the electrodes' stability through long cycles. However, since the potential does not change linearly with time during discharge, equation 1 can only provide an approximate specific capacitance value. Another way to estimate the more accurate specific capacitance value for pseudo-capacitive electrodes is to calculate from CV curves. Equation 2 was utilized to calculate the specific capacitance values from the CV curves**,** and the results are presented in Figure 5-b.

$$C_s = \frac{\int_{V1}^{V2} I(V)dV}{mv(V2 - V1)} \tag{2}$$

$\int_{V1}^{V2} \boldsymbol{I}(\boldsymbol{V})\boldsymbol{dV}$: area under CV curve, $\boldsymbol{m}$: mass of active material (g), $\boldsymbol{v}$: scan rate (V/s)

It is seen from Figure 5-b that the highest specific capacitance value of 8.28 F/g was obtained at 5 mV/s, and as expected, it gradually decreases with increasing scan rate. The lowest specific capacitance value calculated from the CV curves was found to be 6.9 F/g, which is slightly higher than the specific capacitance calculated from the GCD discharge curve.

In summary, it can be noted from the electrochemical analysis results that synthesized FeB-B_4C composite powders have the potential to be a candidate for supercapacitor applications with a pseudocapacitive charge storage behavior. The capacitive performance can be further increased by decreasing particle size, increasing specific surface area, improving the FeB:B_4C phase ratio, and optimizing the cell conditions such as electrolyte type and molarity.

4. CONCLUSION

In this study, FeB-B_4C composite powder without any residual phases, such as graphite, boron oxide, or iron oxide, was synthesized by one-pot sol-gel technique at 1500°C. The morphological inspections showed that a composite of elongated boron carbide particles and sub-micron sized spherical FeB particles formed. The electrochemical properties of the synthesized composite powder investigated by three-electrode set-up. The pseudo-capacitive behavior of electrodes was revealed from the observed oxidation/reduction peaks and potential oblique in the cyclic voltammogram and discharge profiles of electrodes, respectively. The highest specific capacitance value of 8.28 F/g was calculated from the CV curves at a scan rate of 5 mV/s. The synthesized FeB-B_4C composite powder can be used as an active material for fabricating positive electrodes for supercapacitors. The performance of electrodes can be improved by optimizing the particle size and phase ratio.

ACKNOWLEDGEMENTS

The author is grateful for the financial support from The Scientific and Technological Research Council of Turkey (TUBITAK) and Yıldız Technical University under contract numbers of 120M651 and FBA-2023-5301, respectively.

CONFLICT OF INTEREST

The author stated that there are no conflicts of interest regarding the publication of this article.

REFERENCES

[1] Zandalinas SI, Fritschi FB, Mittler R. Global Warming, Climate Change, and Environmental Pollution: Recipe for a Multifactorial Stress Combination Disaster. Trends in Plant Science 2021;26(6):588–99.

[2] Simons S, Schmitt J, Tom B, Bao H, Pettinato B, Pechulis M. Chapter 10 - Advanced concepts. In: Brun K, Allison T, Dennis R (editors). Thermal, mechanical, and hybrid chemical energy storage systems. London: Academic Press, an imprint of Elsevier; 2021. p. 569–96.

[3] Olabi AG, Abbas Q, Al Makky A, Abdelkareem MA. Supercapacitors as next generation energy storage devices: Properties and applications. Energy 2022;248:123617.

[4] Sanger A, Kumar A, Kumar A, Jain PK, Mishra YK, Chandra R. Silicon Carbide Nanocauliflowers for Symmetric Supercapacitor Devices. Ind. Eng. Chem. Res. 2016;55(35):9452–8.

[5] Liu W, Soneda Y, Kodama M, Yamashita J, Hatori H. Low-temperature preparation and electrochemical capacitance of WC/carbon composites with high specific surface area. Carbon 2007;45(14):2759–67.

[6] Halim J, Kota S, Lukatskaya MR, Naguib M, Zhao M-Q, Moon EJ, Pitock J, Nanda J, May SJ, Gogotsi Y, Barsoum MW. Synthesis and Characterization of 2D Molybdenum Carbide (MXene). Adv. Funct. Mater. 2016;26(18):3118–27.

[7] Shiota I, Miyamoto Y (editors). Functionally grated materials 1996. Amsterdam: Elsevier; 1997.

[8] Avcıoğlu S, Kaya F, Kaya C. Morphological evolution of boron carbide particles: Sol-gel synthesis of nano/micro B4C fibers. Ceramics International 2021;47(19):26651–67.

[9] Song S, Yu L, Ruan Y, Sun J, Chen B, Xu W, Zhang J-G. Highly efficient Ru/B4C multifunctional oxygen electrode for rechargeable Li O2 batteries. Journal of Power Sources 2019;413:11–9.

[10] Song S, Xu W, Zheng J, Luo L, Engelhard MH, Bowden ME, Liu B, Wang C-M, Zhang J-G. Complete Decomposition of Li2CO3 in Li-O2 Batteries Using Ir/B4C as Noncarbon-Based Oxygen Electrode. Nano Lett 2017;17(3):1417–24.

[11] Song N, Gao Z, Zhang Y, Li X. B4C nanoskeleton enabled, flexible lithium-sulfur batteries. Nano Energy 2019;58:30–9.

[12] Wang H, Ma C, Yang X, Han T, Tao Z, Song Y, Liu Z, Guo Q, Liu L. Fabrication of boron-doped carbon fibers by the decomposition of B4C and its excellent rate performance as an anode material for lithium-ion batteries. Solid State Sciences 2015;41:36–42.

[13] Luo W-B, Chou S-L, Wang J-Z, Liu H-K. A B 4 C nanowire and carbon nanotube composite as a novel bifunctional electrocatalyst for high energy lithium oxygen batteries. J. Mater. Chem. A 2015;3(36):18395–9.

[14] Luo L, Chung S-H, Yaghoobnejad Asl H, Manthiram A. Long-Life Lithium-Sulfur Batteries with a Bifunctional Cathode Substrate Configured with Boron Carbide Nanowires. Adv Mater 2018;30(39):e1804149.

[15] Chang Y, Sun X, Ma M, Mu C, Li P, Li L, Li M, Nie A, Xiang J, Zhao Z, He J, Wen F, Liu Z, Tian Y. Application of hard ceramic materials B4C in energy storage: Design B4C@C core-shell nanoparticles as electrodes for flexible all-solid-state micro-supercapacitors with ultrahigh cyclability. Nano Energy 2020;75:104947.

[16] Avcıoğlu S, Buldu-Akturk M, Erdem E, Kaya F, Kaya C. Boron Carbide as an Electrode Material: Tailoring Particle Morphology to Control Capacitive Behaviour. Materials (Basel) 2023;16(2).

[17] Avcıoğlu C, Avcıoğlu S, Bekheet MF, Gurlo A. Photocatalytic Overall Water Splitting by SrTiO 3 Progress Report and Design Strategies. ACS Appl. Energy Mater. 2023;6(3):1134–54.

[18] Avcıoğlu C, Avcıoğlu S, Bekheet MF, Gurlo A. Solar hydrogen generation using niobium-based photocatalysts: design strategies, progress, and challenges. Materials Today Energy 2022;24:100936.

[19] Wang D, Song Y, Zhang H, Yan X, Guo J. Recent advances in transition metal borides for electrocatalytic oxygen evolution reaction. Journal of Electroanalytical Chemistry 2020;861:113953.

[20] Yang HX, Wang YD, Ai XP, Cha CS. Metal Borides: Competitive High Capacity Anode Materials for Aqueous Primary Batteries. Electrochem. Solid-State Lett. 2004;7(7):A212.

[21] Zhang L, Chai S-S, Zhang W-B, Guo S-B, Han X-W, Guo Y-W, Bao X, Ma X-J. Cobalt boride on clay minerals for electrochemical capacitance. Applied Clay Science 2022;218:106416.

[22] Li J, Lin H, Chen Y, Su Q, Huang Q. The effect of iron oxide on the formation of boron nitride nanotubes. Chemical Engineering Journal 2011;174(2-3):687–92.

[23] Kriegesmann J. 2.04 - Processing of Silicon Carbide-Based Ceramics. In: Sarin VK, Mari D, Llanes L, Nebel CE (editors). Comprehensive hard materials. Amsterdam, Waltham: Elsevier; 2014. p. 89–175.

[24] Avcıoğlu S, Buldu M, Kaya F, Kaya C. Chapter 20 - Synthesis of nuclear-grade nano-sized boron carbide powders and its application in LDPE matrix composites for neutron shielding. In: Low I-M, Dong Y (editors). Composite materials: Manufacturing, properties, and applications. Amsterdam, Netherlands: Cambridge, MA; Elsevier; 2021. p. 543–79.

[25] Avcıoğlu S, Buldu M, Kaya F, Üstündağ CB, Kam E, Menceloğlu YZ, Kaptan HY, Kaya C. Processing and properties of boron carbide (B4C) reinforced LDPE composites for radiation shielding. Ceramics International 2020;46(1):343–52.

[26] Avcioglu S, Kaya F, Kaya C. Effect of elemental nano boron on the transformation and morphology of boron carbide (B4C) powders synthesized from polymeric precursors. Ceramics International 2020;46(11):17938–50.

[27] Ramachandran R, Xuan W, Zhao C, Leng X, Sun D, Luo D, Wang F. Enhanced electrochemical properties of cerium metal-organic framework based composite electrodes for high-performance supercapacitor application. RSC Adv 2018;8(7):3462–9.

[28] Hadji F, Omari M, Mebarki M, Gabouze N, Layadi A. Zinc doping effect on the structural and electrochemical properties of LaCoO3 perovskite as a material for hybrid supercapacitor electrodes. Journal of Alloys and Compounds 2023;942:169047.

[29] Yavuz A, Ozdemir N, Erdogan PY, Zengin H, Zengin G, Bedir M. Nickel-based materials electrodeposited from a deep eutectic solvent on steel for energy storage devices. Appl. Phys. A 2019;125(8):1–10.